ACS APPLIED MATERIALS & INTERFACES

Research Article

www.acsami.org

Honeycomb-like Porous Carbon–Cobalt Oxide Nanocomposite for High-Performance Enzymeless Glucose Sensor and Supercapacitor Applications

Rajesh Madhu,*[,†,⊥] Vediyappan Veeramani,[†,⊥] Shen-Ming Chen,*[,†] Arumugam Manikandan,[‡] An-Ya Lo,[#] and Yu-Lun Chueh[‡]

[†]Department of Chemical Engineering and Biotechnology, National Taipei University of Technology, Taipei 10608, Taiwan

[‡]Department of Materials Science and Engineering, National Tsing Hua University, Hsinchu, Taiwan

[#]Department of Chemical and Materials Engineering, National Chin-Yi University of Technology, Taichung, Taiwan

Supporting Information

ABSTRACT: Herein, we report the preparation of Pongam seed shells-derived activated carbon and cobalt oxide (~2–10 nm) nanocomposite (PSAC/Co_3O_4) by using a general and facile synthesis strategy. The as-synthesized PSAC/Co_3O_4 samples were characterized by a variety of physicochemical techniques. The PSAC/Co_3O_4-modified electrode is employed in two different applications such as high performance nonenzymatic glucose sensor and supercapacitor. Remarkably, the fabricated glucose sensor is exhibited an ultrahigh sensitivity of 34.2 mA mM^{-1} cm^{-2} with a very low detection limit (21 nM) and long-term durability. The PSAC/Co_3O_4 modified stainless steel electrode possesses an appreciable specific capacitance and remarkable long-term cycling stability. The obtained results suggest the as-synthesized PSAC/Co_3O_4 is more suitable for the nonenzymatic glucose sensor and supercapacitor applications outperforming the related carbon based modified electrodes, rendering practical industrial applications.

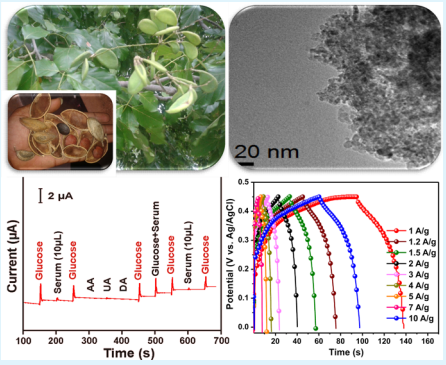

KEYWORDS: *pongam seed shells, activated carbon, cobalt oxide nanoballs, electrochemical glucose biosensor, supercapacitor*

INTRODUCTION

In recent decades, biomass derived porous carbon materials have been shown to be imperative to construct environment-friendly energy storage devices and ultrahigh performance sensors.[1−3] Diabetes mellitus is a group of metabolic diseases, and it is highly responsible for several major health problems. Hence, the diagnosis of glucose determination is domineering, and several approaches have been devoted to construct glucose biosensors based on the glucose oxidase enzyme. However, the enzyme immobilization on the electrode surface is one of the most challenging tasks, and it is highly affected by temperature, pH, and humidity, which causes poor stability.[4−6] Based on the above-mentioned problems, nonenzymatic glucose sensors have been widely explored and developed. As evidenced, graphene based metal oxides, such as NiO/$Ni(OH)_2$, CuO, ZnO, and Co_3O_4/$Co(OH)_2$), exhibit higher sensitivity, lower detection limits for nonenzymatic glucose sensors, as well as remarkable supercapacitor performance with high specific capacitance and excellent energy density, which is necessary for energy storage applications.[3,5,7,8] In particular, cobalt oxide nanocomposites have been attracted due to their enhanced electrocatalytic behavior and good chemical stability, and they have been extensively used in supercapacitors and enzyme-free glucose sensor applications.[3,8−15] As is well-known, the preparation of graphene from graphite is a complicated task which may lead to an hazardous explosion during the oxidation of graphite. Besides, the procedure for the preparation of ACs is simple, eco-friendly, and cost-effective, which leads to possession of unique properties, such as higher surface area, modulated pore size, lower toxicity, excellent chemical stability, and presence of oxygen surface functional groups naturally.[1,2,15−17] Nonetheless, the availability of literature reports on biomass-derived ACs for the electrochemical applications is scarce. Moreover, pongam tree parts are widely used as efficient antibiotics, and also used to cure several types of skin and health problems. In particular, pongam seed shells are natural biomass, abundant, and easily available, and there is no report available for the preparation of activated carbon used as precursor.

Fascinatingly, we report the preparation of pongam seed shells derived activated carbon (PSAC), and PSAC/Co_3O_4 nanocomposite for the first time. Owing to the outstanding physicochemical properties of Pongam seed shells activated carbon (PSAC), we first sought to explore the electrochemical performances of PSAC/Co_3O_4 nanocomposites in two different potential applications: sensitive enzyme-free glucose biosensor

Received: April 1, 2015
Accepted: June 30, 2015
Published: June 30, 2015

DOI: 10.1021/acsami.5b04132
ACS Appl. Mater. Interfaces 2015, 7, 15812−15820

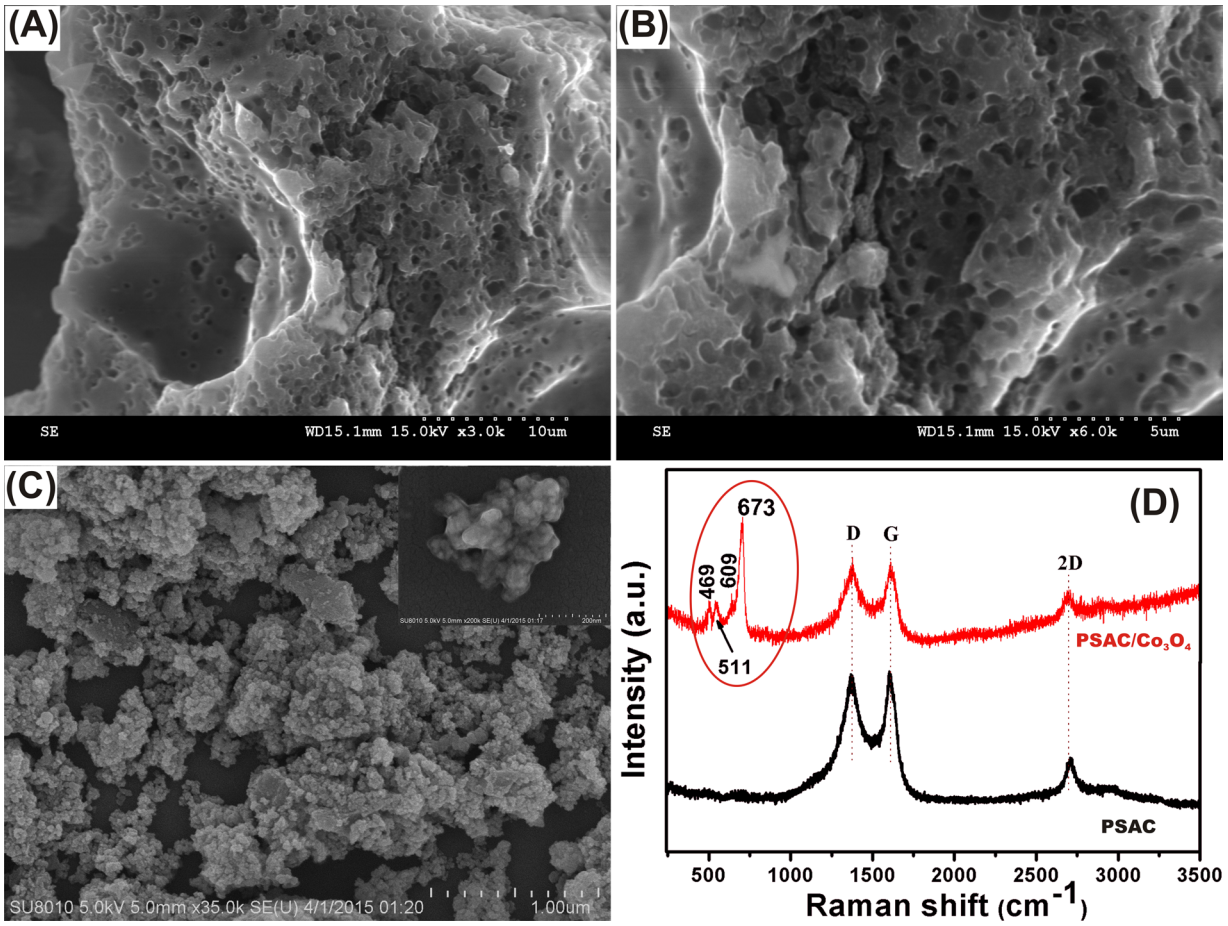

Figure 1. (A,B) SEM images of PSAC, (C) SEM images of PSAC/CO_3O_4 nanocomposite. Inset: Higher magnification image of PSAC/CO_3O_4. (D) Raman spectra of PSAC and PSAC/CO_3O_4.

and supercapacitor applications. Herein, a PSAC/Co_3O_4-modified glassy carbon electrode (GCE) is used for the enzyme-free glucose sensor, which exhibits remarkable analytical parameters, viz. favorable lower overpotential, low detection limits, and ultrahigh sensitivity. In addition, the fabricated supercapacitor offers a good specific capacitance and long-term stability, which surpasses that of several carbon based materials.

RESULTS AND DISCUSSION

Figure 1A,B displays the SEM images of the as-synthesized PSAC samples at different magnifications, which demonstrates the honeycomb-like structure highly porous morphology. Furthermore, Figure 1C shows the SEM image of the PSAC/Co_3O_4 nanocomposite sample; as can be seen, the Co_3O_4 are in the sphere form, and they are firmly covered by carbon layers with the porous nature (inset of Figure 1C). The XRD patterns of the as-synthesized PSAC and PSAC/Co_3O_4 samples are shown in the inset of Figure S1. As shown, the XRD pattern of PSAC demonstrates the two broad diffraction peaks at 23° and 43°, which correspond to the (002) and (101) plane reflection, and it reveals the amorphous behavior of graphitic carbon.[1] The XRD spectrum of PSAC/Co_3O_4 represents the positions, and the relative intensity diffraction peaks at 2θ values denote the pure face centered cubic (fcc) phase of the spinel Co_3O_4 structure with average crystallite size about ∼12 nm and lattice constant 0.8018 nm, which is in good agreement with the literature values (JCPDS 42-1467).[3,18] In addition, no impurity peaks are observed, signifying the high purity behavior of the as-prepared PSAC/Co_3O_4 nanocomposite.

Figure 1D depicts the Raman spectra of the PSAC and PSAC/Co_3O_4 samples, while PSAC possesses two characteristic peaks at 1340 and 1590 cm^{-1} corresponding to the disordered carbon of the D band and E_2g mode phonons of the sp^2 graphitic carbon G band, respectively. The nanocomposite PSAC/Co_3O_4 exhibits four additional peaks (469, 511, 609, 673), which related to the vibrational modes of crystalline Co_3O_4 Eg, $F2g^1$, $F2g^2$, and Ag^1, respectively. Furthermore, the intensity ratio (I_D/I_G) of the PSAC value is 0.99, and PSAC/Co_3O_4 nanocomposites have 1.01, which is nearly the same as that for PSAC and which may be due to the existence of Co_3O_4 nanoparticles on the PSAC surface. The above morphological and structural characterization results evident the fruitful hybridization of PSAC/Co_3O_4 nanocomposite.

Further characterization by high resolution-transmission electron microscopy (HR-TEM) displays the honeycomb-like mesoporous structure of PSAC (Figure 2A) and formation of PSAC/Co_3O_4 nanocomposite at different magnifications (Figure 2B–D).

Obviously, the Co_3O_4 nanoparticles with diameter ranging from 2 to 10 nm (relatively similar to XRD results) were well-dispersed in the worm-like mesoporous structure. In addition, the HRTEM image shows the lattice distance around 2.43 Å, which corresponds to the (311) plane. The growth mechanism of the PSAC/Co_3O_4 nanocomposite is proposed based on the observed experimental results. Scheme 1 shows the schematic

DOI: 10.1021/acsami.5b04132
ACS Appl. Mater. Interfaces 2015, 7, 15812−15820

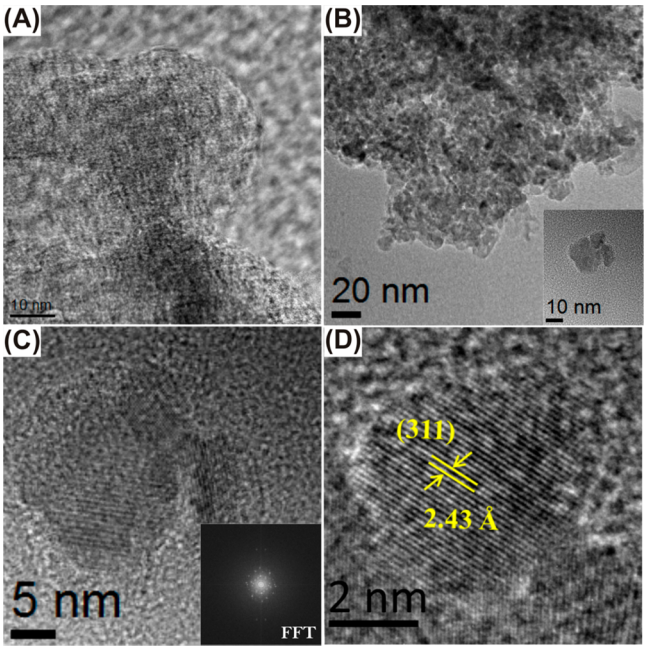

Figure 2. (A) Hr-TEM images of PSAC. (B–D) PSAC/Co_3O_4 nanocomposite at various magnifications.

illustration for the formation of Co_3O_4 nanoparticles on the surfaces of PSAC. Briefly, the specific surface area (SSA) (~700 $m^2\ g^{-1}$), with the highly porous nature of PSAC, has been prepared by using a general and simple KOH activation method using cost-free and abundant biological waste, i.e. pongam seed-shells. In agreement with our previous reports,[1,2] during the activation process, large pore volumes and oxygen containing functional groups were formed on the PSAC surface. The proposed mechanism can be written as[18,19]

$$6KOH + 2C \rightarrow 2K + 3H_2 + 2K_2CO_3 \quad (1)$$

$$K_2CO_3 \rightarrow K_2O + CO_2 \quad (2)$$

$$K_2CO_3 \rightarrow 2C + 2K_2O \quad (3)$$

$$K_2O + C \rightarrow 2K + CO \quad (4)$$

The KOH activation is highly necessary to increase the surface area and create the pores, and also it helps to form the various oxygen surface functional groups, as discussed in our recipe report in detail.[1,2] Mainly, these groups, such as hydroxyl (C–OH) and carbonyl/quinone (C=O), were possibly involved in the formation of Co_3O_4 nanoparticles anchored on the negatively charged PSAC surface, as shown in Figure S2 and Figure 3. The desired molar concentration of $CoCl_2$ was added to the black color PSAC solutions and the Co^{2+} ions which selectively bonded with epoxy and hydroxyl groups through the electrostatic interactions.

The presence of the oxygen functional groups on the negatively charged PSAC has a higher capability to absorb the positively charged metal ions (i.e., Co^{2+}) via electrostatic interactions and to act as nucleation sites. The Co^{2+} ions were easily diffuse and prefer the $Co(OH)_2$ on the PSAC surface. After hydrothermal treatment, $Co(OH)_2$ was turned into Co_3O_4 nanoparticles and started crystallization growth along with the surface of PSAC. As a result, the Co_3O_4 nanoparticles were formed on the surface of PSAC support during the hydrothermal reaction. Hence, the larger amount of functional groups act as an electron-donating source to provide a larger amount with smaller size of nanoparticles on the PSAC surface.

Furthermore, XPS survey spectra (Figure 3A) of the PSAC/Co_3O_4 sample display the corresponding peaks of carbon, oxygen, and Co_3O_4. Figure 3B–D shows the enlarged view of the XPS spectra of C 1s, O 1s, and Co $2P_{3/2}$, and the $2P_{1/2}$ orbit of the PSAC/Co_3O_4 nanocomposite at the binding energies of 284, 529.6, 780.24, and 795.52 eV, respectively.[2,20] In the enlarged view of the C 1s region, we observed 4 peaks at 283.82, 284.5, 285.6, and 287.4 eV, which correspond to the C–H, C–C, C–OH, and carbonyl/quinone groups (C=O), respectively. Similarly, O 1s exhibits 4 peaks: 529.5 and 530.3, assigned to carbonyl/quinone (C=O); 531.4 and 532.6, assigned to carbonate structures on the surface; and hydroxyl and ethers (C–OH, C–O–C), respectively. Figure 3D represents the core level spectra for Co $2p_{3/2}$ orbitals' fitted four peaks (Figure 3D). The binding energies (BEs) of 779.5 and 785.6 eV represent the Co^{3+} and its satellite line, and the BEs of 781.1 and 789.7 eV relate to Co^{2+} and its satellite line.[21]

To investigate the surface area and pore size distribution of the as-prepared PSAC and PSAC/Co_3O_4 samples, we analyzed Brunauer–Emmett–Teller (BET) N_2 adsorption–desorption isotherms at 77 K, and the obtained results are shown in Figure S3. In agreement with previous reports, the observed typical Type-IV curves denote that the existence of mesopores was revealed at P/P_0 in the range of 0.45–0.9. Compared to the pure-PSAC (700 $m^2\ g^{-1}$, 0.47 $cm^3\ g^{-1}$), the PSAC/Co_3O_4 (164 $m^2\ g^{-1}$, 0.34 $cm^3\ g^{-1}$) nanocomposite exhibits a lower surface area and pore volume, as expected because of the integration of Co_3O_4.

As shown in Figure S5, Co_3O_4-free PSAC-modified GCE does not show any corresponding glucose redox peaks, and only Co_3O_4 modified GCE shows a small response with a featureless redox peak. Besides, with the introduction of Co_3O_4 on the PSAC surface, we observed two pairs of redox peaks with enhanced peak currents. In addition, once the 1 mM glucose added into the 0.1 M NaOH, the corresponding

Scheme 1. Schematic Illustration for the Formation of Co_3O_4 Nanoparticles on the Honeycomb-like Porous Surface of PSAC

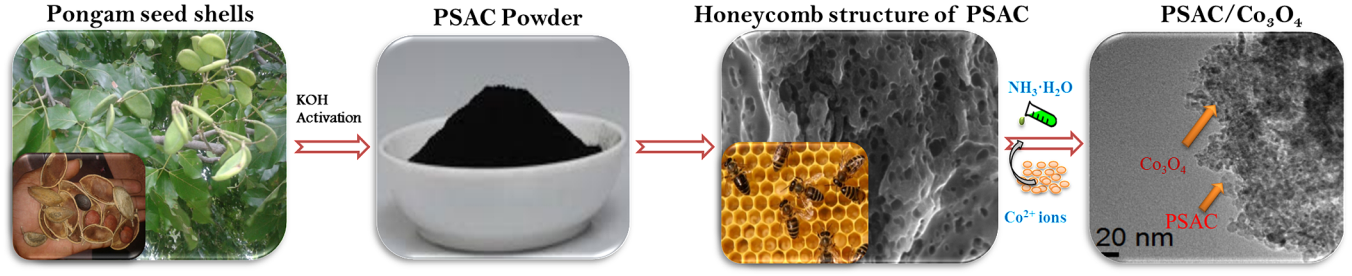

DOI: 10.1021/acsami.5b04132
ACS Appl. Mater. Interfaces 2015, 7, 15812–15820

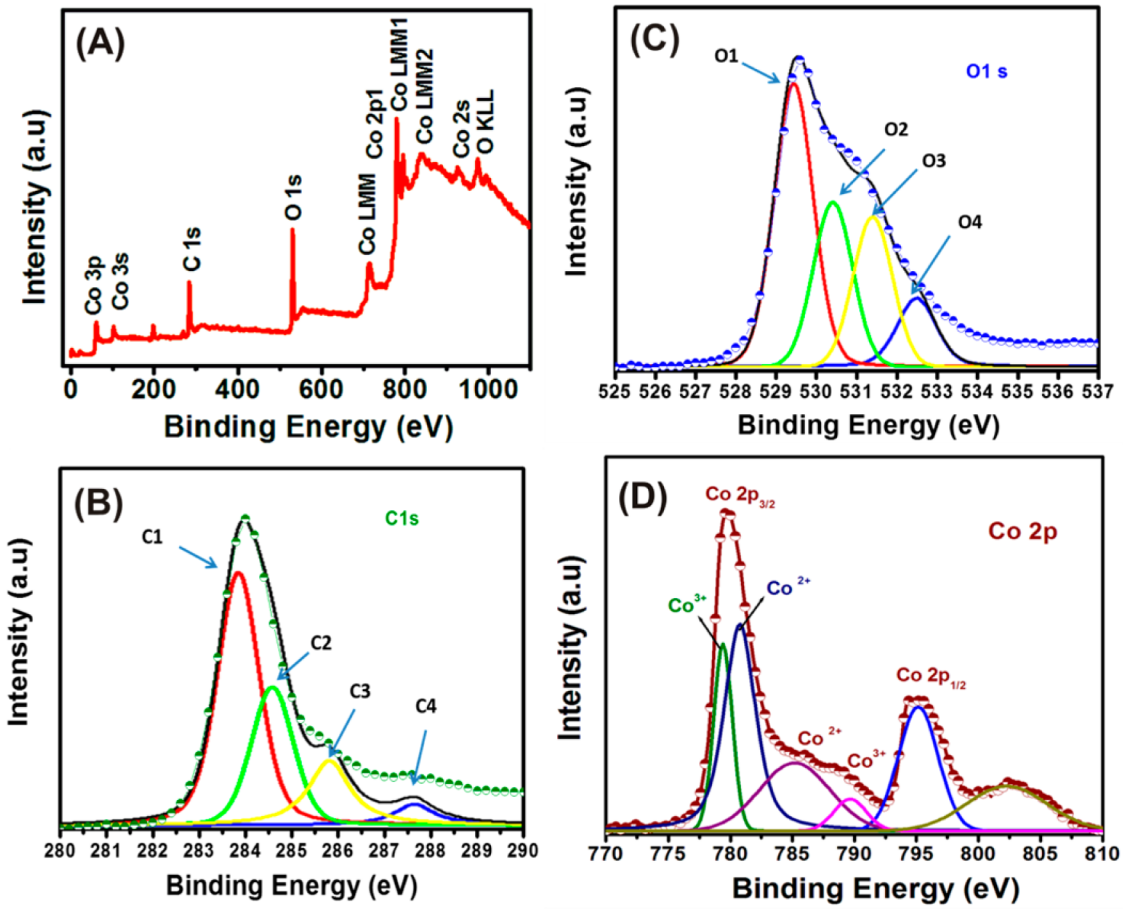

Figure 3. (A) XPS survey spectra of PSAC/Co_3O_4 nanocomposite. (B–D) XPS core level spectra of C 1s, O 1s, and Co 2p of PSAC/Co_3O_4 nanocomposite.

oxidation peak currents of glucose were obviously increased (eqs 5 and 6). Figure 4A demonstrates the CVs of the PSAC/Co_3O_4 at different scan rates in the range 10–100 mV/s in the presence of 1 mM glucose in 0.1 M NaOH. Interestingly, we observed two pairs of redox peaks of (I/II) corresponding to the reversible transition between Co_3O_4 and CoOOH, and (III/IV) reveals the transition between CoOOH and CoO_2. Notably, we achieved significantly lower oxidation potentials at 0.1 V (I) and 0.47 V (III), surpassing the several carbon based-cobalt nanocomposite electrodes.[3,7,8,22−25] The possible reaction mechanism can be expressed in eqs 5 and 6

$$Co_3O_4 + OH^- + H_2O_3 \leftrightarrow CoOOH + e^- \quad (5)$$

$$CoOOH + OH^- \leftrightarrow CoO_2 + H_2O + e^- \quad (6)$$

The redox peak currents were significantly increased with increasing scan rates in Figure S6 (A and B), which suggests a surface-controlled electrochemical process. As shown in Figure 4B, the glucose oxidation peak currents (III) were increased linearly with the increasing glucose concentration up to 3.3 mM (R^2 = 0.9808), and the peak currents remained constant. The obtained result is more consistent with Ding's report,[23] revealing the electrooxidation of glucose is mainly mediated by CoOOH/CoO_2 rather than Co_3O_4/CoOOH in alkaline solution.[3,23] The superior results may be attributed to the synergistic effect between the as-synthesized PSAC and Co_3O_4 nanospheres, which includes the high surface area and modulated pore sizes with high-energy adsorption sites (BET) for the glucose oxidation provided by the fast electron transfer channel offered by a simple eco-friendly fabrication method.

To attain the higher sensitivity, we have performed the amperometric i-t experiments at a PSAC/Co_3O_4 nanocomposite modified electrode with the successive addition of glucose at different concentrations in 0.1 M NaOH solution (*app.* potential +0.55 V) as shown in Figure 4c. Fascinatingly, we obtained a wide linear range from 0.05 to 22004 μM, and the linear equation can be expressed as I (μA) y = 2.7038x ($\pm$0.063) + 2.7081 (R^2=0.9969) (inset to Figure 4c). The calculated detection limit and sensitivity are 21 nM and 34.2 μA mM^{-1} cm^{-2}, respectively. Remarkably, we achieved a very low detection limit and ultrahigh sensitivity toward detection of glucose, which surpass those of the several carbon-based nanocomposite electrodes (Table 1).

To study the stability performance of a nonenzymatic glucose sensor, 50 consecutive CV cycles were recorded in the absence and presence of 1 mM glucose in 0.1 M NaOH. Fascinatingly, no obvious peak current changes were observed. Furthermore, we have performed the long-time stability of the reported glucose sensor in 1 mM glucose in 0.1 M NaOH, and its oxidation peak current response was monitored periodically. The sensor retains about 97.2% of its initial oxidation peak current response after 2 weeks in air at room temperature, revealing the good stability of the modified electrode for glucose determination. In order to assess the reproducibility, 6 independent modified electrodes were prepared for the determination of 1 mM glucose in 0.1 M NaOH, which

DOI: 10.1021/acsami.5b04132
ACS Appl. Mater. Interfaces 2015, 7, 15812−15820

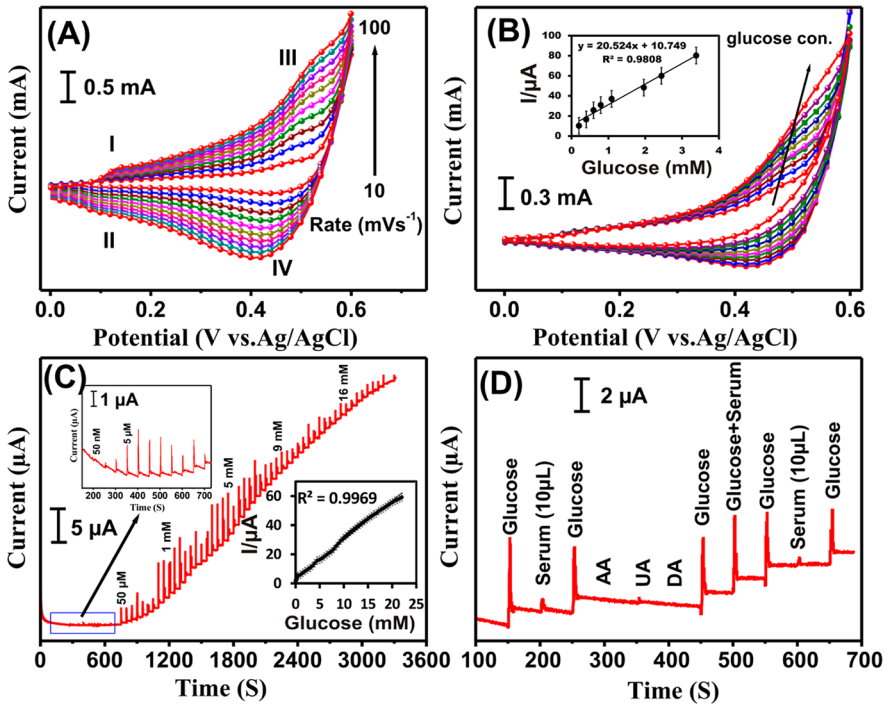

Figure 4. (a) CVs obtained at PSAC/Co_3O_4-modified GCE at different scan rates in the presence of 1 mM glucose. (b) CV curves at various concentrations of glucose (0−3.3 mM) at the scan rate of 50 mV s^{-1}. (c) Typical amperometric response of PSAC/Co_3O_4-modified GCE at different concentrations of glucose (0.05−22004 μM) and corresponding calibration plot (inset). (d) Influence of electroactive interferences (0.5 mM AA, 0.1 mM UA, 0.1 mM DA, and serum (10 μL) with and without glucose) on the response of 0.1 mM glucose. Supporting electrolyte: 0.1 M NaOH saturated with nitrogen gas; *app.* potential: +0.55 V.

Table 1. Comparison of Analytical Parameters for Detection of Glucose over Various Modified Electrodes

Electrodes	Linear range (mM)	Detection limit (μM)	Sensitivity (μA mM^{-1} cm^{-2})	ref
graphene−Co_3O_4 needle electrode	0.050 to 300	<10		3
3D Graphene-Cobalt Oxide	up to 0.080	<25 nM	3390	8
Cobalt oxide nanoparticles	0.7 to 60	0.15	2515.35	10
Electrospun Co_3O_4 nanofibers/Nafion/GCE	up to 2.04	0.97	36.25	23
Ni−Co NSs/RGO/GCE	0.010 to 2.65	3.79	1773.61	24
layered cobalt carbonate hydroxide (LCCH)/FTO	up to 3.5	0.058	571.8	25
Mesoporous $Ni_{0.3}Co_{2.7}O_4$	0.001 to 2.55	1	0.206	26
Cobalt oxide/MWCNTs	0.15 to 5	70		27
PSAC/CO_3O_4	0.05 μM to 22 mM	0.02	34.23	This work

exhibited a satisfactory reproducibility with a relative standard deviation (RSD) of 2.7%. In addition, the repeatability for 5 successive measurements with the RSD of 3.2% for the determination of 1 mM glucose in 0.1 M NaOH reveals a good repeatability of the proposed sensor. Furthermore, the real-time application and specificity are the most important parameters for the glucose sensor. Figure 4D demonstrates the selectivity behavior of the PSAC/Co_3O_4 nanocomposite for the glucose sensor, and it is inactive toward ascorbic acid, uric acid, dopamine (common contaminants in the blood), and 10 μL of glucose-free serum sample (contains a large variety of proteins and other molecules). Besides, we observed an enhanced peak current response for the addition of serum (10 μL) mixed glucose. Hence, the obtained results indicate that the PSAC/Co_3O_4 modified electrode is vastly useful for glucose detection in real samples in the presence of foreign species. The PSAC/Co_3O_4 modified GCE was further tested for the detection of glucose in human blood serum and urine samples (collected from a healthy man) by a standard addition method with same experimental conditions for three time measurements of each sample. In both the cases, a good response is observed, as summarized in Table S2. The superior recoveries of the enzyme-free glucose sensor in real samples designate that the PSAC/Co_3O_4 modified electrode is indeed reliable even in practical applications.

Additionally, we employed the as-synthesized PSAC/Co_3O_4 nanocomposite for the supercapacitor application. Figure 5a shows the CVs of PSAC, Co_3O_4, and PSAC/Co_3O_4 electrodes over a voltage range of 0 to 0.5 V at the scan rate of 20 mV s^{-1} in 1 M KOH electrolyte. For a PSAC modified electrode, we observed a small oxidation peak around 0.3 V with rectangular behavior, which corresponded to the presence of the oxygen functional groups carbonyl (C═O), hydroxyl (C−OH), and ethers (C−OH, C−O−C), in agreement with XPS results.[25,26] Fascinatingly, we observed a superior redox peak current area of the CV curve with the introduction of Co_3O_4 on the PSAC surface. The approximate specific capacitance values are 20, 47, and 80 F g^{-1} for PSAC, Co_3O_4, and PSAC/Co_3O_4, respectively, which reveals that the specific capacitance was increased by pseudocapacitance of the PSAC/Co_3O_4 nanocomposite. More-

DOI: 10.1021/acsami.5b04132
ACS Appl. Mater. Interfaces 2015, 7, 15812−15820

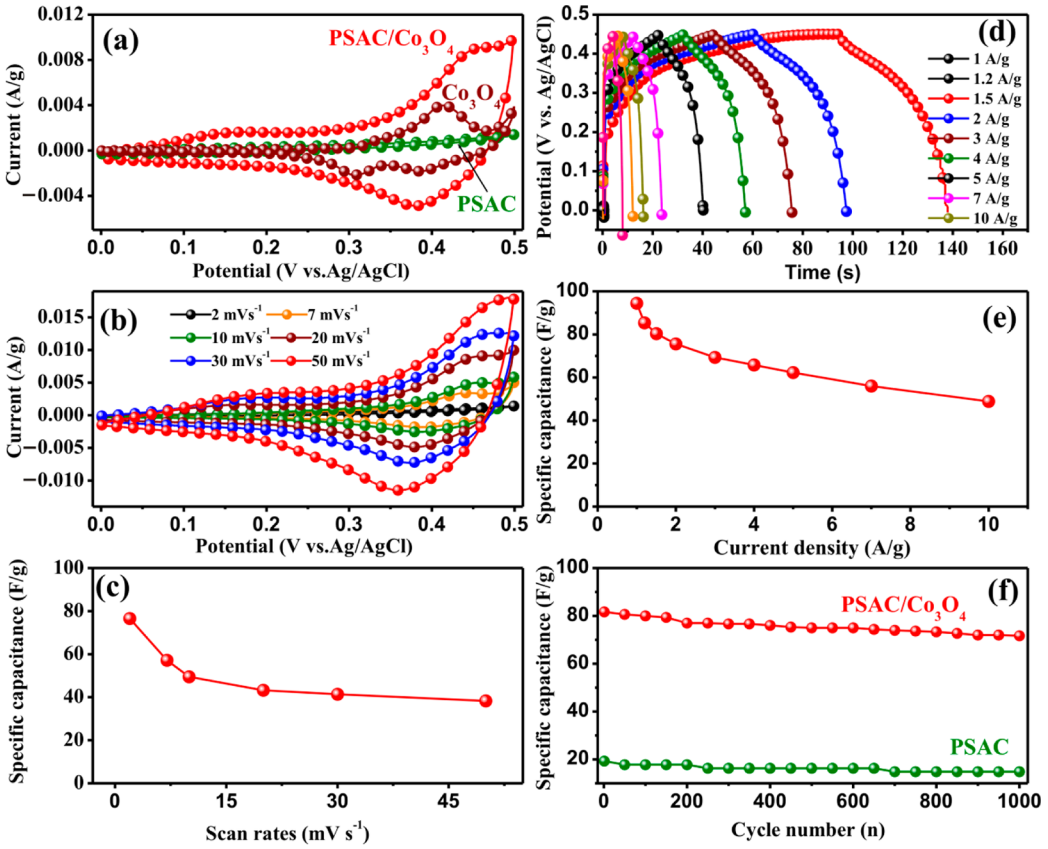

Figure 5. Electrochemical properties of PSAC/Co_3O_4-modified electrodes measured using a three-electrode system in 1.0 M KOH aqueous electrolyte. (a) The comparative CV curves for the PSAC, Co_3O_4, and PSAC/Co_3O_4 electrodes at 20 mV s^{-1}. (b) CV curves obtained at the PSAC/Co_3O_4 electrode at different scan rates. (c) Calibration plot between different scan rates and specific capacitance. (d) Galvanostatic charge−discharge curves of the PSAC/Co_3O_4 electrode at current densities of 1, 1.2, 1.5, 2, 3, 4, 5, 7, and 10 Ag^{1-}. (e) Calibration plot between current density and specific capacitance. (f) Cycle performance of the PSAC/Co_3O_4 electrode measured at a current density of 1.5 Ag^{1-}.

over, the redox peaks of the CVs (Figure 5b,c) at the PSAC/Co_3O_4 fabricated electrode were maintained even at higher scan rates (2 to 50 mV s^{-1}) using 1.0 M KOH, which further revealed the good electrochemical reversibility, and the redox peak currents are proportional to scan rates, meaning the process is surface controlled. This can be attributed to the pseudocapacitive contribution from the oxygen surface functional groups,[2,26] which can improve the wettability and maximize the electroactive surface area.[25] Figure 5d shows the galvanostatic charge−discharge (GCD) behavior of the PSAC/Co_3O_4 electrode under varied current densities. The approximate specific capacitances of the PSAC/Co_3O_4 electrode are 48, 56, 62, 65, 69, 76, 80, 85, and 94 F/g at the current densities of 10, 7, 5, 4, 3, 2, 1.5, 1.2, and 1 A/g, respectively (Figure 5e). The obtained specific capacitance of our PSAC/Co_3O_4 electrode is quite comparable to those of several reported carbon based electrodes, as shown in Table S2.[8,12−15,28−30]

Figure 5f displays the cyclic stability of the PSAC/Co_3O_4 electrode at a current density of 1.5 A g^{-1} up to 1000 cycles. Interestingly, the specific capacitance of the PSAC/Co_3O_4 electrode only decreases up to 12% of its initial capacitance even after 1000 charge−discharge cycles and stays stable afterward. For comparison, we have performed the charge−discharge experiments at PSAC, PSAC/Co_3O_4 electrodes as shown in Figure S8. For a PSAC electrode, we observed a good capacitive retention, which is more than that of a graphene electrode,[31] while, with the introduction of Co_3O_4 on the PSAC surface, the GCD profiles were observed with a small potential plateau with higher capacitance and even after long-term cycles. For the practical applications, capacitive retention is more important in several portable electronic power tools and vehicles. In general, when the discharge current density is higher for the electrode with a lower specific capacitance is due to the occurrence of Faradaic reaction resistance and ion diffusion resistance. Hence, the obtained results establish that our PSAC/Co_3O_4 electrode has provided a good specific capacitance and cycle stability, outstanding the several carbon based cobalt oxide nanocomposite electrodes.

In addition, we have performed electrochemical spectroscopy (EIS) experiments to analyze the electrochemical kinetics at the electrode/electrolyte interface. The Nyquist plots obtained from PSAC and PSAC/Co_3O_4 samples (Figure 6) show a well-defined semicircle in the high−medium frequency region accompanied by a vertical line in the low frequency region, which is more consistent with several previous reports.[32] As known, the semicircle in the higher frequency region denotes the equivalent series resistance (ESR), and it is a combination of solution resistance and intrinsic resistance of the active material, which occurs by the ionic conductivity of the electrolyte ions, and it consists of a parallel combination of the constant phase element (CPE) and a series of interfacial resistance and current collector.

Moreover, the diameter of the semicircle signifies the charge transfer resistance at electrode/electrolyte interfaces. Compared to the PSAC, the PSAC/Co_3O_4 material displayed a

DOI: 10.1021/acsami.5b04132
ACS Appl. Mater. Interfaces 2015, 7, 15812−15820

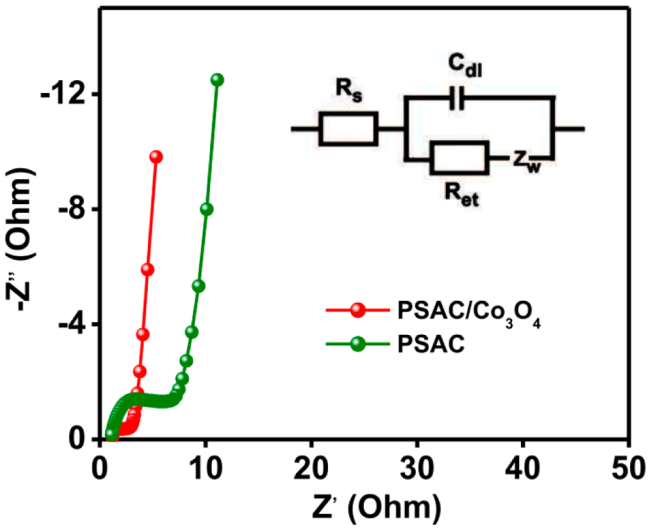

Figure 6. Nyquist plots observed for the PSAC and PSAC/Co_3O_4 samples.

lower charge transfer resistance, because of the synergistic effect between the PSAC and Co_3O_4 components.[32] Hence, the obtained analytical parameters suggest that the PSAC/Co_3O_4 nanocomposite is a promising electrode material for nonenzymatic glucose sensors and supercapacitors, rendering practical industrial applications.

CONCLUSIONS

In summary, PSAC/Co_3O_4 nanocomposite is synthesized by using a simple and eco-friendly method. Notably, the as-synthesized nanocomposite offers a remarkable performance toward the reported enzyme-free glucose sensor and supercapacitor application. The achieved electrochemical performance may be ascribed to the catalytic activity of the Co_3O_4 with a strong substrate of high surface area PSAC materials, which can be used for practical industrial applications.

EXPERIMENTAL METHODS

Materials. Potassium hydroxide, sodium hydroxide, cobalt chloride hexahydrate ($CoCl_2 \cdot 6H_2O$), and ethanol were purchased from Sigma-Aldrich. Ammonium hydroxide water ($NH_3 \cdot H_2O$) and HCl were purchased from J.T. BAKER Chemicals. All the chemicals were used without further purification. The experiments were carried out by using doubly distilled water.

Synthesis of PSAC/CO_3O_4 nanocomposite. The high-surface-area (~700 m^2 g^{-1}), with the highly porous nature of PSAC, was prepared by using a general and simple KOH activation method using no cost and abundant biological waste, i.e. pongam seed-shells (*Pongamia pinnata*). Briefly, the sun-dried pongam seed-shells were washed and then dried in an oven at 100 °C. The pulverized seed-shells were precarbonized at 350 °C for 2 h in a N_2 flow tubular furnace; the collected precarbonized black solid was added to 10% of KOH solution under N_2 flow while stirring at 80 °C. The activated slurry was placed in an open atmosphere for 24 h and subsequently transferred into a quartz crucible at 900 °C (optimum) for 2 h in a N_2 atmosphere at a heating rate of 5 °C min^{-1} in a tube furnace. The carbonized samples were washed with HCl (5%) and double-distilled water until the pH became neutral, and they were dried at 100 °C for 24 h to remove the moisture and thoroughly ground to yield the finest carbon powder.

The PSAC/CO_3O_4 nanocomposite was synthesized by using a simple and eco-friendly method. The PSAC/Co_3O_4 nanocomposites were prepared by a hydrothermal method. In this process, 30 mg of PSAC powder was suspended in 30 mL of deionized water by ultrasonic dispersion for 30 min to form a black color solution, and the supernatant was collected for further processing. Further, 30 mM $CoCl_2$ was dropped into 30 mL of supernatant PSAC solutions and stirred for 50 min. Subsequently, the aqueous solution of ammonium hydroxide water ($NH_3 \cdot H_2O$) was added dropwise into the above suspension until the pH of the solution reached 10. Finally, the mixed solution was transferred to the Teflon-lined stainless steel autoclave. The autoclave was put in an oven at 200 °C for 12 h and slowly cooled down to room temperature naturally. The black color precipitate was obtained and washed with several times with ethanol followed by water. The as-prepared PSAC/Co_3O_4 nanocomposites were obtained after being dried at 70 °C under a vacuum. Finally, the resulting samples were calcined at 250 °C for 5 h under an argon atmosphere.

Materials Characterization. The surface morphology of the film was studied using JEOL field-emission scanning electron microscopy, and the nanostrucutres were examined by field emission transmission electron microscopy (FE-TEM, JEM-3000F, JEOL operated at 300 kV for high resolution-transmission electron microscopy (HR-TEM)). X-ray diffraction (XRD) was performed on a Rigaku, MiniFlex II instrument. The Raman spectra were recorded at ambient temperature using a WITeck CRM200 confocal microscopy Raman system with a 488 NM laser. N_2 adsorption−desorption isotherms and the pore size distribution were studied using "Micromeritics ASAP 2020". For the X-ray photoelectron spectroscopy, a "XPS ULVAC-PHI PHI 5000 VersaProbe" was used.

Preparation of Modified Electrodes. For the electrochemical nonenzymatic glucose sensor, the as-synthesized PSAC/CO_3O_4 sample was first dispersed in ethanol under sonication treatment for 2 h. Meanwhile, the surface of the GCE was carefully polished; ca. 6 μL of dispersed PSAC (with optimal concentration, see Figure S7) was drop cast on the GCE, followed by drying in an air oven at 30 °C.

In order to prepare the supercapacitor electrode, the as-synthesized PSAC/CO_3O_4 active electrode material, 80 wt % of PSAC/CO_3O_4, 15 wt % of graphite is mixed with 0.4 mL of *N*-methylpyrrolidinone (NMP) to form a homogeneous slurry. Further 15 μL of slurry is coated on the 1 × 1 cm^2 area of the stainless steel electrode by a drop casting method and dried overnight at 60 °C. The mass loading of PSAC/CO_3O_4 on the substrate is 0.8 mg cm^{-2}. The cell was soaked in electrolyte for a few hours before undergoing the electrochemical study.

Electrochemical Measurements. For nonenzymatic glucose sensor applications, CV and Amperometry i-t profiles were recorded by using a electrochemical analyzer (CH instruments, CHI900) at room temperature using a conventional three-electrode cell consisting of a GCE as the working electrode, Ag/AgCl (saturated KCl) as the reference electrode, and a platinum wire as the counter electrode.

For supercapacitor applications, PSAC and PSAC/CO_3O_4 electrodes were assessed by a three electrode system within the potential range of 0 to 0.5 V in 1.0 M KOH electrolyte solution. All the cyclic votammetry (CV) and galvanostatic charge−discharge (GCD) profiles were performed by using the CHI627 electrochemical analyzer. The specific capacitances of the sample electrodes were calculated by using the following equations:[33]

In the case of CV measurements:

$$C = Q/m\Delta V \tag{7}$$

where C signifies the specific capacitance (unit of F g^{-1}), Q is the average charge during the charge−discharge process (unit of C), m is the mass of the active material (unit of g), and ΔV is the working potential (unit V).

For GCD measurements:

$$C = I\Delta t/m\Delta V \tag{8}$$

where I is the current density (unit A) and Δt is the charge/discharge duration (unit s).

DOI: 10.1021/acsami.5b04132
ACS Appl. Mater. Interfaces 2015, 7, 15812−15820

■ ASSOCIATED CONTENT

Supporting Information

BET surface area analysis, BJH pore size distribution, and FTIR spectra CV results. The Supporting Information is available free of charge on the ACS Publications website at DOI: 10.1021/acsami.5b04132.

■ AUTHOR INFORMATION

Corresponding Authors

*E-mail: rajesphysics@gmail.com.
*E-mail: smchen78@ms15.hinet.net.

Author Contributions

⊥R.M. and V.V. contributed equally to this work.

Notes

The authors declare no competing financial interest.

■ ACKNOWLEDGMENTS

Financial support for this work by the Ministry of Science and Technology, Taiwan (NSC101-2113-M-027-001-MY3) to S.M.C. is gratefully acknowledged. The authors thank Mr. Madhu, Farmer, Dharmapuri, Tamilnadu, India for helpful discussion on biowastes and Pongam seed shells collection. A.Y.L. would like to acknowledge the MOST (103-2221-E-167−037 -MY3) for XPS studies.

■ REFERENCES

(1) Madhu, R.; Vijaya Sankar, K.; Chen, S.-M.; Selvan, R. K. Eco-friendly Synthesis of Activated Carbon from Dead Mango Leaves for the Ultrahigh Sensitive Detection of Toxic Heavy Metal Ions and Energy Storage Applications. *RSC Adv.* **2014**, *4*, 1225−1233.

(2) Madhu, R.; Veeramani, V.; Chen, S.-M. Heteroatom-Enriched and Renewable Banana-Stem-derived Porous Carbon for the Electrochemical Determination of Nitrite in Various Water Samples. *Sci. Rep.* **2014**, *4*, 4679.

(3) Wang, X.; Dong, X.; Wen, Y.; Li, C.; Xiong, Q.; Chen, P. A Graphene−Cobalt Oxide based Needle Electrode for Non-enzymatic Glucose Detection in Micro-droplets. *Chem. Commun.* **2012**, *48*, 6490−6492.

(4) Wilson, R.; Turner, A. P. F. Glucose Oxidase-an Ideal Enzyme. *Biosens. Bioelectron.* **1992**, *7*, 165−185.

(5) Kang, X. H.; Mai, Z. B.; Zou, X. Y.; Cai, P. X.; Mo, J. Y. A Sensitive Nonenzymatic Glucose Sensor in Alkaline Media with a Copper Nanocluster/Multiwall Carbon Nanotube-modified Glassy Carbon Electrode. *Anal. Biochem.* **2007**, *363*, 143−150.

(6) Bharath, G.; Madhu, R.; Chen, S. M.; Vediyappan, V.; Balamurugan, A.; Mangalaraj, D.; Viswanathan, C.; Ponpandian, N. Enzymatic Electrochemical Glucose Biosensors by Mesoporous 1D Hydroxyapatite-on-2D Reduced Graphene Oxide. *J. Mater. Chem. B* **2014**, *3*, 1360.

(7) Rakhi, R. B.; Chen, W.; Cha, D.; Alshareef, H. N. Substrate Dependent Self-Organization of Mesoporous Cobalt Oxide Nanowires with Remarkable Pseudocapacitance. *Nano Lett.* **2012**, *12*, 2559−2567.

(8) Dong, X. C.; Xu, H.; Wang, X. W.; Huang, Y. X.; Park, M. B. C.; Zhang, H.; Wang, L. H.; Huang, W.; Chen, P. 3D Graphene Cobalt Oxide Electrode for High-Performance Supercapacitor and Enzyme-less Glucose Detection. *ACS Nano* **2012**, *4*, 3206−3213.

(9) Li, G.; Huo, H.; Xu, C. $Ni_{0.31}Co_{0.69}S_2$ Nanoparticles Uniformly Anchored on a Porous Reduced Graphene Oxide Framework for a High-Performance Non-enzymatic Glucose Sensor. *J. Mater. Chem. A* **2015**, *3*, 4922−4930.

(10) Sattarahmady; Heli, H. A Non-enzymatic Amperometric Sensor for Glucose Based on Cobalt Oxide Nanoparticles. *J. Exp. Nanosci.* **2012**, *7*, 529−546.

(11) Guo, C.; Zhang, X.; Huo, H.; Xu, C.; Han, X. Co_3O_4 Microspheres with Free-standing Nanofibers for High Performance Non-Enzymatic Glucose Sensor. *Analyst* **2013**, *138*, 6727−6731.

(12) Liu, H.; Gou, X.; Wang, Y.; Du, X.; Quan, C.; Qi, T. Cauliflower-Like Co_3O_4/Three-Dimensional Graphene Composite for High Performance Supercapacitor Applications. *J. Nanomater.* **2015**, Article ID 874245.

(13) Wu, C.; Shen, Q.; Mi, R.; Deng, S.; Shu, Y.; Wang, H.; Liu, J.; Yan, H. Three-Dimensional Co_3O_4/Flocculent Graphene Hybrid on Ni Foam for Supercapacitor Applications. *J. Mater. Chem. A* **2014**, *2*, 15987−15994.

(14) Patil, U.; Lee, S. C.; Kulkarni, S.; Sohn, J. S.; Nam, M. S.; Han, S.; Jun, S. C. Nanostructured Pseudocapacitive Materials Decorated 3D Graphene Foam Electrodes for Next Generation Supercapacitors. *Nanoscale* **2015**, *7*, 6999−7021.

(15) Ma, L.; Zhou, H.; Shen, X.; Chen, Q.; Zhu, G.; Ji, Z. Facile Synthesis of Co_3O_4 Porous Nanosheets/ Reduced Graphene Oxide Composites and their Excellent Supercapacitor Performance. *RSC Adv.* **2014**, *4*, 53180−53187.

(16) Sevilla, M.; Fuertes, A. B. Direct Synthesis of Highly Porous Interconnected Carbon Nanosheets and Their Application as High Performance Supercapacitors. *ACS Nano* **2014**, *8*, 5069−5078.

(17) Sevilla, M.; Mokaya, R. Energy Storage Applications of Activated Carbons: Supercapacitors and Hydrogen Storage. *Energy Environ. Sci.* **2014**, *7*, 1250−1280.

(18) Madhu, R.; Veeramani, V.; Chen, S. M.; Palanisamy, J.; Ezhil Vilian, A. T. Pumpkin Stem-derived Activated Carbons as Counter Electrodes for Dye-sensitized Solar Cells. *RSC Adv.* **2014**, *4*, 63917−63921.

(19) Qie, L.; Chen, W.; Xu, H.; Xiong, X.; Jiang, Y.; Zou, F.; Hu, X.; Xin, Y.; Zhang, Z.; Huang, Y. Synthesis of Functionalized 3D Hierarchical Porous Carbon for High-Performance Supercapacitors. Energy. *Energy Environ. Sci.* **2013**, *6*, 2497−2504.

(20) Wang, J.; Kaskel, S. KOH Activation of Carbon-Based Materials for Energy Storage. *J. Mater. Chem.* **2012**, *22*, 23710−23725.

(21) Zhang, L.; He, W.; Xiang, X.; Li, Y.; Li, F. Roughening of Windmill-Shaped Spinel Co_3O_4 Microcrystals Grown on a Flexible Metal Substrate by a Facile Surface Treatment to Enhance their Performance in the Oxidation of Water. *RSC Adv.* **2014**, *4*, 43357−43365.

(22) Shim, H. W.; Lim, A. H.; Kim, J. C.; Jang, E.; Seo, S. D.; Lee, G. H.; Kim, T. D.; Kim, D. W. Scalable One-pot Bacteria-templating Synthesis Route toward Hierarchical, Porous-Co_3O_4 Superstructures for Supercapacitor Electrodes. *Sci. Rep.* **2013**, *3*, 2325.

(23) Ding, Y.; Wang, Y.; Su, L.; Bellagamba, M.; Zhang, H.; Lei, Y. Electrospun Co_3O_4 Nanofibers for Sensitive and Selective Glucose Detection. *Biosens. Bioelectron.* **2010**, *26*, 542−548.

(24) Wang, L.; Lu, X.; Ye, Y.; Sun, L.; Song, Y. Nickel-Cobalt Nanostructures Coated Reduced Graphene Oxide Nanocomposite Electrode for Nonenzymatic Glucose Biosensing. *Electrochim. Acta* **2013**, *114*, 484−493.

(25) Kung, C. W.; Lin, C. Y.; Lai, Y. H.; Vittal, R.; Ho, K. C. Cobalt Oxide Acicular Nanorods with High Sensitivity for the Non-enzymatic Detection of Glucose. *Biosens. Bioelectron.* **2011**, *27*, 125−131.

(26) Liu, Y.; Zhang, Y.; Wang, T.; Qin, P.; Guo, Q.; Pang, H. Mesoporous $Ni_{0.3}Co_{2.7}O_4$ Hierarchical Structures for Effective Non-enzymatic Glucose Detection. *RSC Adv.* **2014**, *4*, 33514−33519.

(27) Buratti, S.; Brunetti, B.; Mannino, S. Amperometric Detection of Carbohydrates and Thiols by using a Glassy Carbon Electrode Coated with Co Oxide/Multi-wall Carbon Nanotubes Catalytic System. *Talanta* **2008**, *76*, 454−457.

(28) Guan, Q.; Cheng, J.; Wang, B.; Ni, W.; Gu, L. X.; Huang, L.; Yang, G.; Nie, F. Needle-like Co_3O_4 Anchored on the Graphene with Enhanced Electrochemical Performance for Aqueous Supercapacitors. *ACS Appl. Mater. Interfaces* **2014**, *6*, 7626−7632.

(29) Dai, M.; Song, L.; LaBelle, J. T.; Vogt, B. D. Ordered Mesoporous Carbon Composite Films Containing Cobalt Oxide and Vanadia for Electrochemical Applications. *Chem. Mater.* **2011**, *23*, 2869−2878.

DOI: 10.1021/acsami.5b04132
ACS Appl. Mater. Interfaces 2015, 7, 15812−15820

(30) Wang, H. W.; Hu, Z. A.; Chang, Y. Q.; Chen, Y. L.; Zhang, Z. Y.; Yang, Y. Y.; Wu, H. Y. Preparation of Reduced Graphene Oxide/Cobalt Oxide Composites and their Enhanced Capacitive Behaviors by Homogeneous Incorporation of Reduced Graphene Oxide Sheets in Cobalt Oxide Matrix. *Mater. Chem. Phys.* **2011**, *130*, 672−679.
(31) Wu, M. S.; Lin, Y. P.; Lin, C. H.; Lee, J. T. Formation of Nano-Scaled Crevices and Spacers in NiO-attached Graphene Oxide Nanosheets for Supercapacitors. *J. Mater. Chem.* **2012**, *22*, 2442−2448.
(32) Sankar, K. V.; Selvan, R. K. The Ternary $MnFe_2O_4$/ Graphene/Polyaniline Hybrid Composite as Negative Electrode for Supercapacitors. *J. Power Sources* **2015**, *275*, 399−407.
(33) Lu, X.; Zheng, D.; Zhai, T.; Liu, Z.; Huang, Y.; Xie, S.; Tong, Y. Facile Synthesis of Large-area Manganese Oxide Nanorod Arrays as a High-Performance Electrochemical Supercapacitor. *Energy Environ. Sci.* **2011**, *4*, 2915−2921.

DOI: 10.1021/acsami.5b04132
ACS Appl. Mater. Interfaces 2015, 7, 15812−15820